Prog Artif Intell (2018) 7:1–14
https://doi.org/10.1007/s13748-017-0134-4

REGULAR PAPER

A pixel processing approach for retinal vessel extraction using modified Gabor functions

Sameena Pathan[1] · **P. C. Siddalingaswamy**[1] · **K. Gopalakrishna Prabhu**[2]

Received: 25 June 2017 / Accepted: 18 August 2017 / Published online: 29 August 2017

Abstract Computerized image analysis methods for retinal imaging are primarily of great interest and benefit as it provides significant information about the retinal vessels. Retinal image analysis techniques can be of pertinence for ophthalmologists and a stand-alone warning implement for determining the retinal disorders. This requires dedicated image processing algorithms to provide mathematical description about the region of interest. This paper presents an automated pixel processing-based retinal vessel extraction algorithm using modified Gabor functions and morphological operators. Color normalization is performed to make the algorithm adaptable to intra- and inter-image variabilities. Furthermore, the enhanced retinal vessels are subjected to automatic thresholding for vessel pixel classification. The proposed method is tested on a set of retinal images collected from the DRIVE database and subjected to robust performance analysis to evaluate the efficacy. The proposed algorithm achieved an average accuracy of 97.22%, sensitivity of 85.12% and specificity of 98.57%, which is comparably preferable to the well-known algorithms.

Keywords Gabor filter · GLCM · Morphology · Optic disk · Vessel extraction

✉ Sameena Pathan
sameena.pathan.k@gmail.com

P. C. Siddalingaswamy
pcs.swamy@manipal.edu

K. Gopalakrishna Prabhu
gk.prabhu@manipal.edu

[1] Department of Computer Science and Engineering, Manipal Institute of Technology, Manipal University, Manipal, India

[2] Department of Biomedical Engineering, Manipal Institute of Technology, Manipal University, Manipal, India

1 Introduction

A standout among the most vital components in the eye is the retina, consisting of delicate and finely layered nerve cells which line the inside of the eye. The investigation and detection of retinal vessels is basic in diagnosing and distinguishing retinal infections, for example, diabetic retinopathy (DR), hypertension, cardiovascular ailment and so forth. Contrasts in retinal vessel distances across, lengths, tortuosity, reflectivity and edges are imperative estimations deciding the retinal phenotypes of the disease. In clinical ophthalmology, color retinal images acquired are used for the detection and diagnosis of diseases related to eye. Applications of retinal images also include diagnosing regions with no blood vessels, biometric applications, etc. DR is a main source of vision loss in age groups 20–74. In the year 2014, there were around 422 million individuals diagnosed with diabetes. The impact is significantly more declared in Africa with two-thirds of individuals stay undiscovered. Around, 35% of the general population living with diabetes have some amount of DR and 1 in 10 will build up a visual debilitating from the illness [1]. Blood vessel extraction is the fundamental stride to distinguish and analyze different eye infections.

Recent advancements in digital image processing and computational abilities have made it possible to acquire data from medical images using new and revolutionary methods. Current techniques for extraction of blood vessels are mostly manual, expensive and potentially inconsistent requiring expert intervention to carry out the process. The optic disk which is the most prominent feature present in the fundus image interferes with the extraction of the retinal blood vessel extraction process. Therefore, accurately detecting the optic disk and eliminating it from the region of interest forms a major task in extraction of the vessels. The method used in this paper focusses on extraction and enhancement of the reti-

nal blood vessels from the fundus images. The detection of optic disk and consequently eliminating it from the extracted blood vessels is been integrated as a part of our algorithm. The algorithm uses modified morphological techniques in conjunction with optimized Gabor functions for achieving high accuracy in comparison with that of the highly accurate methods available in the literature.

1.1 Related work

Basically, the segmentation-based methods vary depending on the quality of the images, imaging modality, automatic and semiautomatic and other factors. Post-processing and pre-processing contribute in this regard to overcoming the segmentation-related issues. Few vessel extraction methods apply purely intensity-based pixel processing techniques; examples include thresholding subsequently followed by analyzing the connected components, whereas other techniques include the use of explicit models for vessel contour extraction. In order to segment the retinal vessel, pixel classification-based techniques and vessel tracking-based techniques are deployed.

In pixel classification-based techniques, every pixel in the image is subjected to multiple operations by a two-stage processing technique. Initially, the pixels are enhanced using detection techniques such as morphological, matched filtering, adaptive filtering. The second stage includes centerline operation or vessel thinning for subsequent classification of vessel pixels from the background pixels. Pixel classification techniques are classified in subcategories as multi-scale approaches [2], region growing [3] and ridge-based approaches [4], centerline approaches [5], mathematical morphology-based approaches [2] and matched filtering-based approaches [6,7]. Multi-scale vessel extraction involves pixel operation performed on low- and high-resolution images for larger vessel and fine vessel extraction, respectively. Region growing-based approaches often require post-processing to eliminate over-segmentation effects and often require user intervention for the selection of seed point. Value similarity and spatial proximity are the important segmentation criteria used in region growing-based approaches. The property of detection of ridges in different image modalities due to the invariant nature to affine transformation is exploited in the field of medical image processing. Edge focuses are neighborhood tops toward maximal surface gradient. The vessel extraction based on graph description in addition to operations such as thresholding, determination of object connectivity and thinning procedure is used by the centerline approaches, and these approaches are also termed as skeleton-based approaches. Match-filtering approaches convolve the image with multiple matched filters by designing filters to detect different orientations. The computational load is affected by the convolution kernel size. Top-hat and watershed transforms are often used algorithms for segmentation of vessels using mathematical morphology. Dilation and erosion using structuring elements aids in refining the degree of segmentation results.

Vessel tracking (VT) is the second approach used in segmentation of retinal vessel [8,9]. The difference between VT and pixel classification-based approach is that the latter applies local operators on the vessel region and track, whereas the former applies local operators to the entire image. VT is classified as automated [10] and semiautomated. In semiautomated approach, the algorithm tracks the user-specified seed point and tracks the retinal vessels based on local intensity values, whereas in automated tracking approaches, the seed point is selected automatically by the algorithm. The location of the vessel point for the vessel tracking is obtained by functions such as Gaussian. Tracking techniques produce connected segments in contrast to the pixel-based techniques and are suitable for retinal vessel segmentation.

The pixel processing-based approaches [11] scan the overall possible vessel pixels in the entire image, thereby identifying the vascular structured tree. However, the tradeoff is an increase in the computational cost and processing on larger database requires sophisticated hardware for implementation. The enhancement process may erroneously include the noise and enhance the artifacts as well, thereby reducing the accuracy of vessel segmentation. When computational efficiency and processing speed are a major concern, automated tracking-based approaches are much preferred choice as it exclusively includes the neighborhood pixels, thus reducing the unnecessary processing of entire image pixels. However, discontinuities in the complex vascular branches are not a favored choice for VT approaches. Depending on the application requirements, the segmentation approaches can be tailored suitably.

The optic nerve head or plate is the distal bit of the optic nerve stretching out from myelinated bit of nerve starting behind the sclera to the retinal surface. On a normal, the plate vertical width is 1500 μm with a marginally more noteworthy variety in nearsighted eye and lesser variety in the hypermetropic eye. The fact that the blood vessels converge into the optic disk is exploited for extraction of the optic disk from the retinal image. Because of the interruption of the veins in the optic circle, the level of computational complexity increases in retinal vessel segmentation. A few researchers have attempted to address this issue. Aquino et al. [12] presented a methodology for segmenting the optic disk from the retinal images using morphology and edge detection techniques. The optic disk circumference is estimated by circular Hough transform. Morales et al. [13] used mathematical morphology and principal component analysis (PCA). Image inpainting was used for eliminating the blood vessels, and variations of watershed transforms were

applied subsequently. Alshayeji et al. [14] used gravitational law-based edge detection algorithm. Ant colony optimization is used in [15]. In our optic disk removal algorithm, the red channel of the fundus image is utilized due to the predominant visual effect of the optic disk in the red channel image. Histogram equalization and a series of morphological operations using a well-specified structuring element are used. A heuristic threshold is selected such that the error of eliminating the blood vessels is minimized.

1.2 Objective

This paper presents a pixel processing-based approach for designing an automatic and quick retinal vessel extraction algorithm using modified Gabor functions and GLCM-based thresholding techniques. Morphological operators are used for extraction of optic disk and elimination from the region of interest. Despite its simplicity, the algorithm developed produces better results for images of varying inter- and intra-image variabilities. This fact is mainly relevant with the end goal of using the algorithm for integration in developing systems for automated assessment of eye disorders.

The paper organization is as follows. The blood vessel extraction and optic disk elimination is explained in Sect. 2. Section 3 gives the exhaustive depiction of the results and comparative analysis. The conclusions drawn are presented in Sect. 4.

2 Methods

In order to develop a retinal vessel extraction algorithm, the primary task is to obtain effectual database. Forty images provided by DRIVE database are collected [16]. The database also consists of manual labeled retinal vessels used as gold standard. The overall proposed methodology is illustrated in Fig. 1. A two-stage pre-processing is applied to increase the blood vessels extraction accuracy. In the initial stage, the artifacts due to illumination variation is being corrected. In the second stage, the contrast is being increased with the fact that retinal images possess a higher contrast at the center and the contrast decreases in the outward direction. The width of the vessels in a standard retinal image is within 40–200 μm. The width varies as moved radially outward from the optic disk. The vessels are approximated by piecewise linear segments. A set of improved Gabor filters exploit the properties of vessels by incorporating tunable frequency and selective orientations. GLCM-based automatic thresholding scheme is used as a subsequent step for extraction of the enhanced vessels. Some unwanted frills in the image are removed by applying modified mathematical morphology functions. Finally, by applying mathematical morphology and mask generation, the vessel extracted retinal image is made free from the optic disk circular retinal border giving an image depicting the vessels prominently.

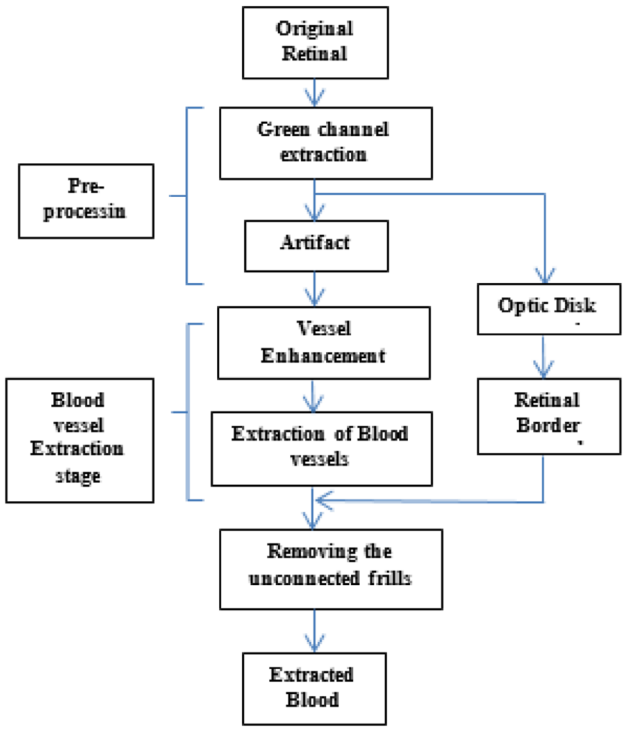

Fig. 1 Overall proposed methodology

2.1 Pre-processing

Practically, a consequential number of images are affected by artifacts such as poor focus, variations in illumination, poor contrast, significant background noise, reflections. The presence of these extraneous variations meddles with the subsequent image analysis process. Capture device variations, reflections, pigmentation differences in retinal images are also contributing factors in this regard. Thus, it is mandatory to filter out these artifacts by pre-processing of the images. Initial step in pre-processing is to reduce such variation by performing color normalization of the original fundus image against a standard reference image. Irrespective of the variations in the captured image, the color normalization is performed using histogram matching, wherein the pixel data are modified such that histogram matches that of the standard reference image. Consider $p_s(x_i)$ and $p_d(x_j)$ as the probability density function of the standard and reference images. The histogram equalization of the standard image is given in (1).

$$T(s) = \int_0^s p_s(x_i)\,dx \tag{1}$$

The histogram equalization is obtained by similar transformation function given in (2).

$$Q(d) = \int_0^d p_{\mathrm{d}}(x_j)\,\mathrm{d}x \tag{2}$$

The values of d for the desired image are obtained as given in (3).

$$d = Q^{-1}[T(s)] \tag{3}$$

This method is applied to images in the database with color variation with respect to the standard reference image. The technique is applied independently to each of the RGB channels. Contrast difference exists at the center and the outer regions of the retinal images, and in order to eliminate the differences and correspondingly increase the contrast, contrast limited adaptive histogram equalization (CLAHE) technique is applied to the image as a second pre-processing technique. The green channel is extracted from the RGB image and used for further processing, since it exhibits higher contrast and exploits the human visual perception by highlighting the retinal vessels prominently.

2.2 Vessel enhancement using optimized Gabor filter parameters

The retinal vessels are usually connected, piecewise linear and prone to noise. Gabor filters are used for image analysis because of their biological significance and computational properties. The kernel of the Gabor wavelet is localized in space and frequency domain. Gabor filters prove to be excellent candidates for retinal vessel detection due to the exhibition of properties such as spatial localization, frequency and orientation selectivity, in addition to quadrature phase relationship. Gabor filters originally introduced by Gabor [17] are obtained by multiplying cosine/sine wave with a Gaussian window as given in (4).

$$g(x) = \left(\frac{1}{\left(\sqrt{2\pi}\right)\sigma}\right) \mathrm{e}^{-\frac{x^2}{2\sigma^2}} \mathrm{e}^{j\omega_o x} \tag{4}$$

where $\left(\frac{1}{\left(\sqrt{2\pi}\right)\sigma}\right) \mathrm{e}^{-\frac{x^2}{2\sigma^2}}$ represents a Gaussian envelope and $\mathrm{e}^{j\omega_o x}$ is a complex sinusoid. ω_o and σ represent the center frequency and spread of the Gaussian window, respectively.

For enhancement of the retinal vessels, the optimized spatial Gabor channel kernels modulation is performed using the Gaussian window. The real part of the corresponding is given in (5).

$$g(x, y) = \exp\left[-\pi\left(\frac{x_p^2}{\sigma_x} + \frac{y_p^2}{\sigma_y}\right)\right] \cos\left(2\pi f x_p\right) \tag{5}$$

where

$$x_p = x\cos\theta + y\sin\theta$$
$$y_p = -x\sin\theta + y\cos\theta$$

θ is the orientation of the filter, f is the passband central frequency. The bandwidth of the filter is determined by σ_x which indicates the standard deviation of Gaussian along the filter in x-direction. The orientation selectivity is determined by σ_y which indicates the standard deviation of Gaussian across the filter in y-direction. The Gabor filter parameters are estimated such that background noise and undesirable structures are eliminated while emphasizing the vessels. The parameters are determined utilizing the procedure in [18] as given in (6–9). The blood vessel width is indicated by thickness parameter t. An appropriate value of t is crucially chosen as the diameter of the blood vessel varies along different directions. A large value of t causes the suppression of the vessels by surrounding noise.

$$f = \frac{0.5}{t} \tag{6}$$

$$\sigma_x = \frac{\lambda_t}{0.75\pi} \tag{7}$$

$$\sigma_y = 0.85\sigma_x \tag{8}$$

$$\lambda = \sqrt{\frac{2ln2}{\pi}} \tag{9}$$

Based on the inferences drawn from manual segmentation, it is observed that the greater number of diameters of vessel are 120 μm wide in a standard fundus image with a resolution of 20 micron/pixel. For enhancing and preserving of the small vessels, the thickness parameter is set to 6. The filter direction and orientation of the Gabor function is determined by angle parameter $\theta \in [0, \pi]$. The real part of the Gabor kernel is depicted in Fig. 2. It can be observed that the Gabor shape is similar to the blood vessel and can be consequently maintained across various orientations. With the choice of these optimal parameters, the Gabor filter is regarded as directional providing directional selectivity. The optimized Gabor filter is applied to the vessel segment as given in (10).

$$r(x, y) = g(x, y) * I_g(x, y) \tag{10}$$

$g(x, y)$ is Gabor filter response and $I_g(x, y)$ is the green channel retinal image. For every pixel position, the green channel image is convolved with the Gabor kernel. The Gabor filter is rotated along different directions in steps of 15° from 0° to 170°, and correspondingly the maximum response is calculated using (11) and the maximum response is retained.

$$r_{\max}(x, y) = \max_\theta [r(x, y)] \tag{11}$$

Fig. 2 Gabor filter real part

In comparison with other angle orientation, maximum response of the vessels is obtained for 0°, 45° and 90°. Figure 3 shows the corresponding response.

2.3 Automatic thresholding and GLCM-based vessel extraction

At the point, after the retinal vessels have been enhanced with respect to the background, the following stride is to extract the vessels. Keeping in mind the end goal to legitimately extricate the improved vessel fragments from the convolved retinal image $r_{\max}(x, y)$, entropy-based thresholding utilizing GLCM is utilized. The GLCM also referred as co-occurrence distribution gives the separation and precise spatial relationship over an image subregion of particular size. The co-occurrence matrix $T = \left[t_{i,j}\right]$ of the image I with $M \times N$ dimensions estimates the transition of gray level intensities between neighboring pixels, thereby finding extreme

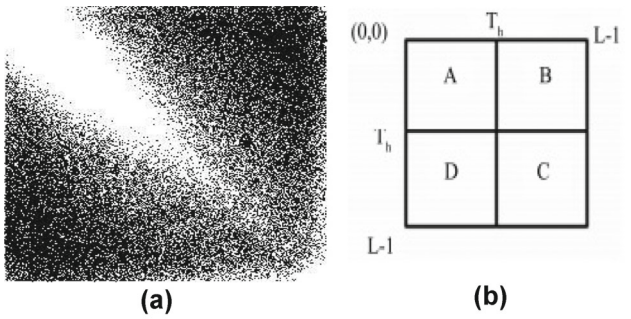

Fig. 4 **a** GLCM gray level distribution. **b** The 4 quadrants of GLCM

usage in determining the threshold value. Consider $f(m, n)$ as the gray level of the image pixel at spatial coordinates (m, n) and the nearest surrounding pixels have gray levels $f(m+1, n)$, $f(m-1, n)$, $f(m, n+1)$, $f(m, n-1)$. By comparing gray levels $f(m, n)$ with all the four neighboring gray levels, the co-occurrence matrix is constructed. Based on the occurrence of gray level i with respect to j, various ways of defining occurrence matrix are possible. Considering horizontally right and vertically lower transitions, the co-occurrence matrix is given by (12)

$$t_{i,j} = \sum_{m=1}^{M} \sum_{n=1}^{N} \delta \tag{12}$$

where

$$\delta = 1 \quad \text{if} \quad \left\{ \begin{array}{c} f(m, n) = i \text{ and } f(m, n+1) = j \\ \text{or} \\ f(m, n) = i \text{ and } f(m+1, n) = j \end{array} \right\}$$

$$\delta = 0 \quad \text{Otherwise}$$

The transition probability from intensity level i to j is obtained as given in (13)

$$P_{i,j} = \frac{t_{i,j}}{\sum_{i=1}^{L} \sum_{j=1}^{L} t_{i,j}} \tag{13}$$

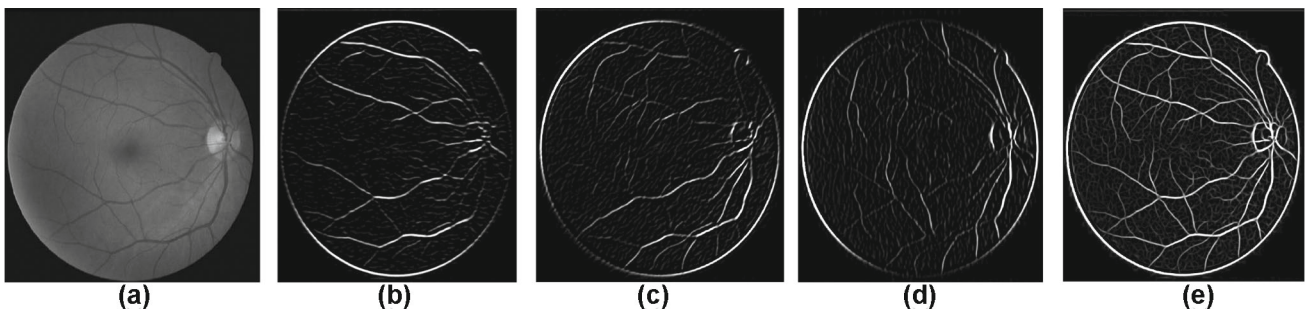

Fig. 3 Images obtained by applying Gabor filter to green channel image at various orientation. **a** Green channel image. **b** Image at orientation of 0°. **c** Image at orientation of 45°. **d** Image at orientation of 90°. **e** Overall Gabor response image

The four quadrants of GLCM and gray level distribution in GLCM are given in Fig. 4. The four quadrants are formed based on the gray level intensity variation within or between object. Considering T_h as the threshold defined in the range $0 \leq T_h \leq L-1$, the quadrants A, B, C and D are partitioned into local and joint quadrant. A and B constitute the local quadrant as the corresponding quadrants indicate the transition within the object and within the boundary, respectively. Similarly, the gray level transition occurring between the region of interest and the image background is indicated by joint quadrants C and D. The quadrants of our interest include A and C, as it helps in estimating the local entropy threshold. P_A and P_C given in (14) and (15) give the object class and background class probabilities.

$$P_A = \sum_{i=0}^{T_h} \sum_{j=0}^{T_h} P_{i,j} \tag{14}$$

$$P_C = \sum_{i=T_h+1}^{L-1} \sum_{j=T_h+1}^{L-1} P_{i,j} \tag{15}$$

The normalized probabilities functions of threshold vector (T_h, T_h) are indicated as $P^A_{i,j}$ and $P^C_{i,j}$ as given in (16) and (17).

$$P^A_{i,j} = \frac{P_{i,j}}{P_A} \tag{16}$$

$$P^C_{i,j} = \frac{P_{i,j}}{P_C} \tag{17}$$

In order to calculate the optimal threshold for extraction of the vessels, the total second-order entropy which constitutes the summation of the individual entropies between the object and background is calculated as given in (18).

$$H_T\left(T_h\right) = H_A\left(T_h\right) + H_C\left(T_h\right) \tag{18}$$

where

$$H_A\left(T_h\right) = -\frac{1}{2} \sum_{i=0}^{T_h} \sum_{j=0}^{T_h} P^A_{i,j} \log_2 P^A_{i,j}$$

$$H_C\left(T_h\right) = -\frac{1}{2} \sum_{i=T_h+1}^{L-1} \sum_{j=T_h+1}^{L-1} P^C_{i,j} \log_2 P^C_{i,j}$$

Ultimately, the optimal threshold indicated as T_E corresponds to maximum value of $H_T\left(T_h\right)$ as shown in (19).

$$T_E = \text{avg}\left[\max_{T=0\ldots L-1} H_T\left(T_h\right)\right] \tag{19}$$

The small unconnected circular objects as seen in Fig. 5a are filtered out by applying the Connected Component labeling algorithm with four neighborhood. This is achieved by application of morphological area opening and circularity conditions taking the value as four for connected components. Consequently, the unnecessary isolated pixels are filtered out as shown in Fig. 5b.

The response to the application of automatic entropy thresholding and connected component labeling to $r_{\max}(x, y)$ is illustrated in Fig. 6. It can be seen that the vessels have been extracted completely.

2.4 Mathematical morphology-based optic disk and border removal

To remove the border, an image $I_m(x, y)$ known as marker image is created using the response image $r_{\max}(x, y)$ as a mask image as given in (20).

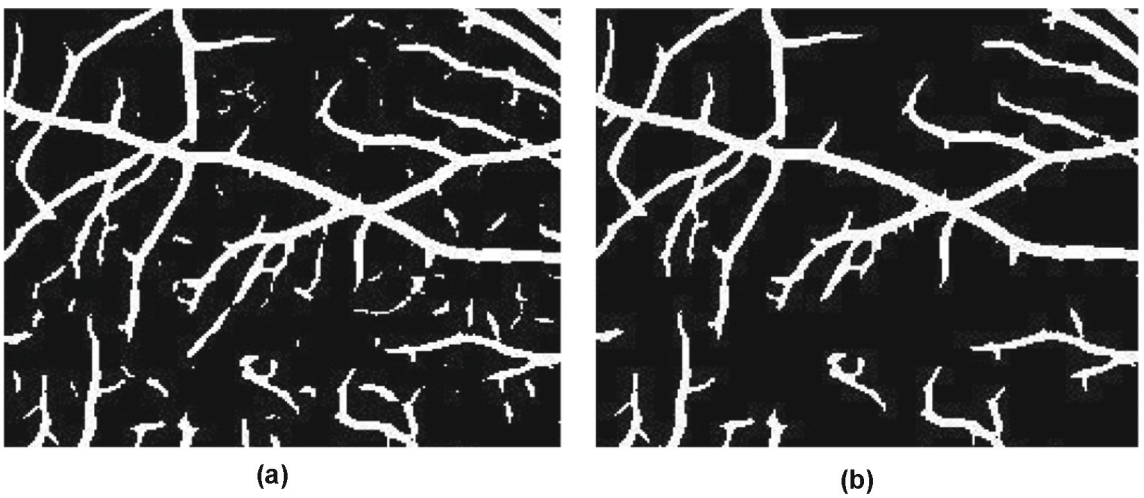

Fig. 5 **a** Small unconnected unwanted components in the response image. **b** After application of CC-labeling algorithm

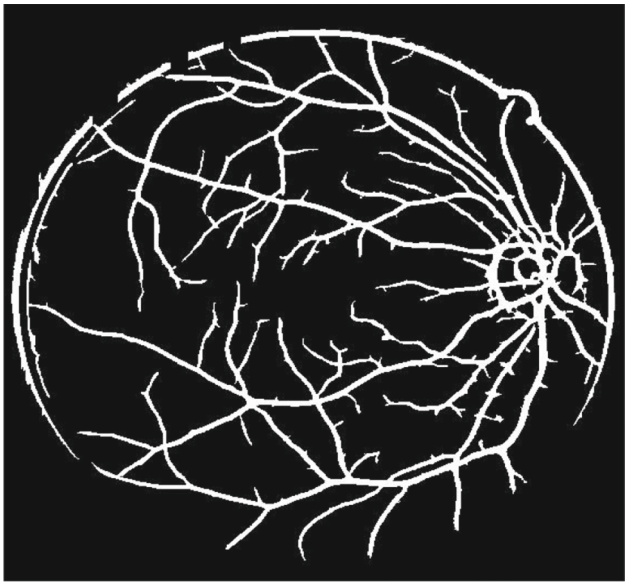

Fig. 6 Extracted vessels from the retinal green channel Image

$$f_{\mathrm{m}}(x, y) = \begin{Bmatrix} r_{\max}(x, y) & \text{if } (x, y) \text{ is on the border} \\ 0, & \text{otherwise} \end{Bmatrix} \quad (20)$$

The marker image $f_{\mathrm{m}}(x, y)$ obtained contains only the objects overlapping with the retinal border. The resultant image containing only the pixels of interest $f_{\mathrm{r}}(x, y)$ is obtained using (21).

$$f_{\mathrm{r}}(x, y) = r_{\max}(x, y) - f_{\mathrm{m}}(x, y) \quad (21)$$

The optic disk shows up as a brilliant spot of roundabout or curved shape, interrupted by active vessels. The optic circle does not have receptors in this layer in the retina, and henceforth it is also known as blind side. To find the optic disk, the red channel of the fundus picture is utilized. It can predominantly be seen in the red channel image because of its prominent luminance property. The red channel image of the fundus is converted to grayscale image $I(x, y)$ with pixel intensity k. The gray level probabilities are given by (22).

$$p_k(r_k) = \frac{n_k}{N} \quad (22)$$

where $0 \leq r_k \leq 1$ and $k = 0, 1, 2 \ldots L-1$, r_k = normalized values for intensities, L = number of image gray levels, n_k = number of pixels of gray level r_k, N = number of pixels in the image.

The plot of $p_k(r_k)$ with respect to r_k is defined as the histogram of the image.

Figure 7a, b shows the image $I(x, y)$ and corresponding histogram. The transformation process that causes the histogram of the image $I(x, y)$ to be uniform is termed as histogram equalization as given by (23).

$$s = T(r) \quad (23)$$

Here, the transformation is single esteemed and monotonically expanding. Numerically, the discrete type of change capacity for histogram equalization is given by (24) [19].

$$s_k = T(r_k) = \sum_{j=0}^{k} \frac{n_j}{N} \quad (24)$$

Figure 7c, d shows the histogram equalized image indicated as $I'(x, y)$ and the corresponding histogram graph. The image obtained by applying histogram equalization indicates that there is dominant peak in the intensity values at the region near the optic disk. In order to localize the optic disk, binarization of the histogram equalized image $I'(x, y)$ is performed. It is quite obvious from the visual inference of Fig. 7c that a higher threshold value close to 1 would yield an image containing optic disk. In our proposed technique, a heuristic threshold of 0.93 is used. Utilizing the defined threshold value, 40 different fundus images were tested and an inference was drawn that 0.93 threshold was appropriate in all cases to a great degree. Binarization process yields two groups of pixels as given in (25).

$$f(x, y) = \begin{Bmatrix} \text{white pixel if } I'(x, y) \geq 0.93 \\ \text{black pixel if } I'(x, y) < 0.93 \end{Bmatrix} \quad (25)$$

The binarized image $f(x, y)$ is convolved with the $f_{\mathrm{r}}(x, y)$ to obtain the blood vessel extracted image $s(x, y)$ with border and optic disk removed. In order to remove the unwanted unconnected pixels introduced during binarization process, morphological opening is applied to $s(x, y)$ as given in (26) using the structuring element se.

$$\mathrm{se} = \begin{matrix} 0\ 1\ 0 \\ 1\ 1\ 1 \\ 0\ 1\ 0 \end{matrix}$$

$$s(x, y) \odot \mathrm{se} = (s(x, y) \ominus \mathrm{se}) \oplus se \quad (26)$$

Suppose H and L represent the Euclidian coordinates of the input image and structuring element, respectively. Consider a region of x, L_x indicating translation of L, and then erosion of image H with L is a set of points x, such that L_x forms a subset of H [20]. Finally, using the concept of morphological opening applied to the image, we get the extricated vessels as shown in Fig. 12e–h. It can be observed that the most challenging task of preserving the thin blood vessels is accomplished.

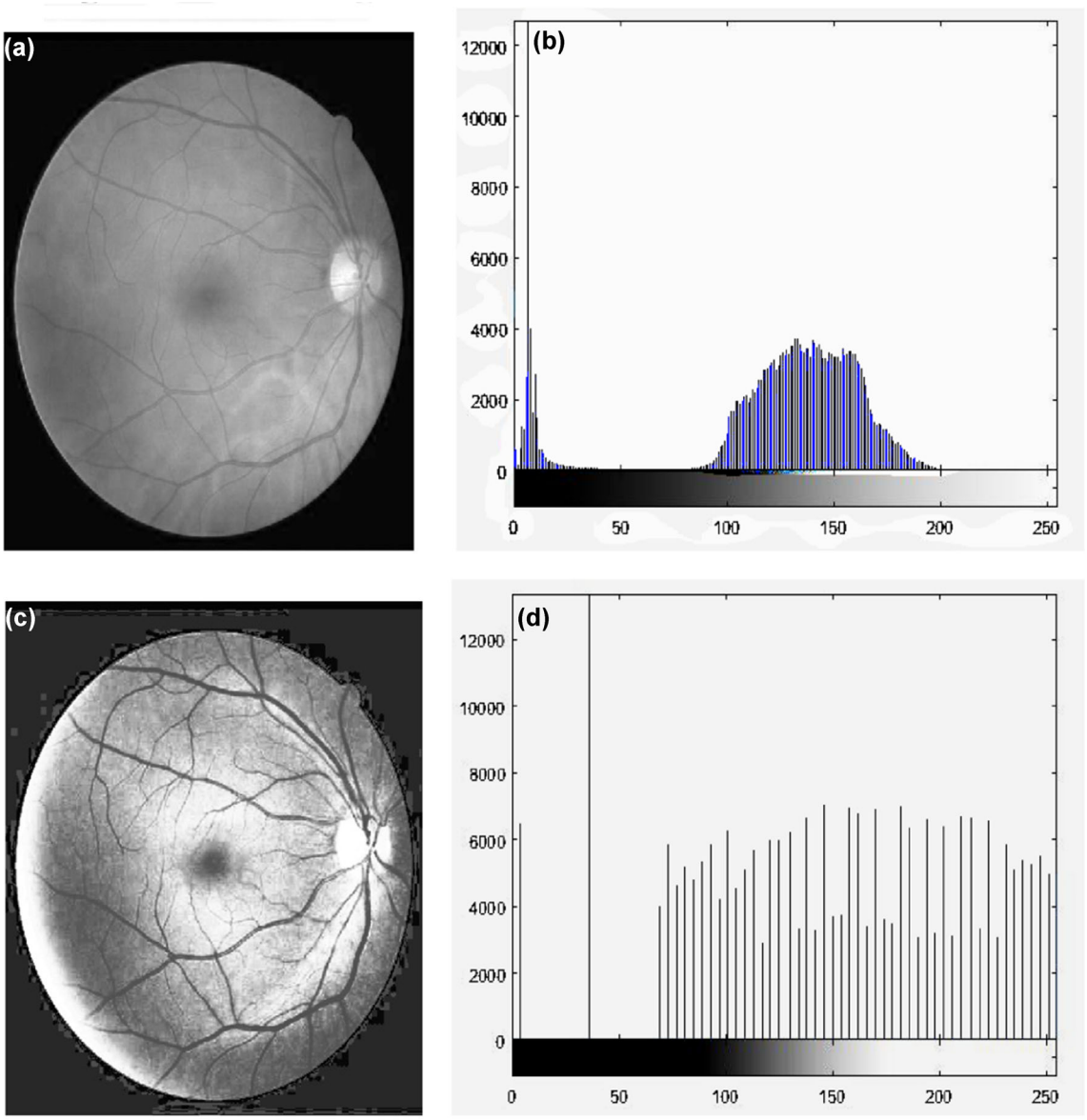

Fig. 7 **a** Image $I(x, y)$. **b** Histogram of image $I(x, y)$. **c** Histogram equalized image $I'(x, y)$. **d** Histogram of the image in **c**

3 Results and discussion

3.1 Evaluation parameters

Peak-signal-to-noise ratio (PSNR) and contrast increase index (CII) are used to evaluate the contrast-enhanced image at the pre-processing stage. The PSNR is calculated as given in (27).

$$\text{PSNR} = 10\log_{10}\frac{\text{MAX}_I^2}{\text{MSE}} \tag{27}$$

where

$$\text{MSE} = \frac{1}{mn}\sum_{i=1}^{m}\sum_{j=1}^{n} \| I_o(i, j) - I_e(i, j)^2 \|$$

MAX indicates maximum intensity of the original image, and the mean squared error between the original and enhanced images is given by MSE. The improvement in contrast is given by contrast improvement index (CI) calculated as the ratio of contrast of enhanced image to contrast of original image given in (28).

$$\text{CI} = \frac{C_{\text{enhanced}}}{C_{\text{original}}} = \frac{x - y}{x + y} \tag{28}$$

x and y indicate the foreground and background mean intensity values. To accurately measure and compare the performance, the gold-standard segmentation result obtained from DRIVE database is used in our study. The performance is evaluated using three metrics, namely sensitivity,

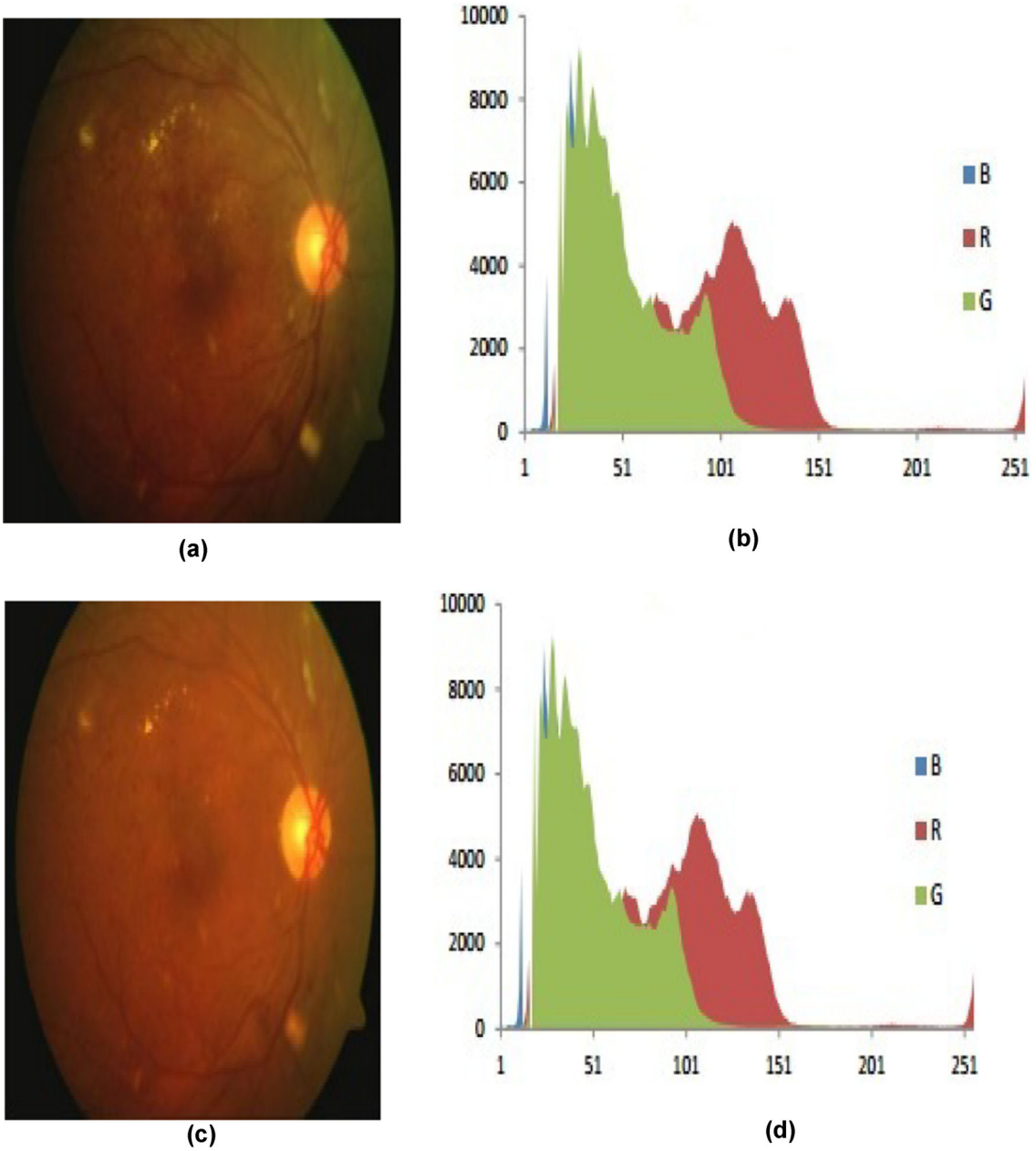

Fig. 8 **a**, **b** Original image and corresponding histogram. **c**, **d** Color-normalized image and corresponding histogram

specificity and accuracy. Sensitivity and specificity represent fraction of pixels correctly classified as vessels and erroneously classified as pixels, respectively. The ratio of total number of pixels correctly classified as blood vessels to the total number of pixels in the image is termed as accuracy. The fraction of pixels erroneously classified as blood vessels is given by false positive rate (FPR). Sensitivity, specificity, accuracy and FPR are calculated as given in (29–32).

$$\text{Sensitivity} = \frac{\text{TP}}{\text{TP} + \text{FN}} \tag{29}$$

$$\text{Specificity} = \frac{\text{TN}}{\text{TN} + \text{FP}} \tag{30}$$

$$\text{Accuracy} = \frac{\text{TP} + \text{TN}}{\text{TP} + \text{FN} + \text{TN} + \text{FP}} \tag{31}$$

$$\text{FPR} = \frac{\text{FP}}{\text{FP} + \text{TN}} \tag{32}$$

TP indicates the pixels which are effectively recognized as vessels. FP indicates the pixels incorrectly recognized as blood vessels. TN indicates the pixels which are effectively recognized as non-blood vessels. FN indicates the pixels which are incorrectly recognized as non-blood vessels.

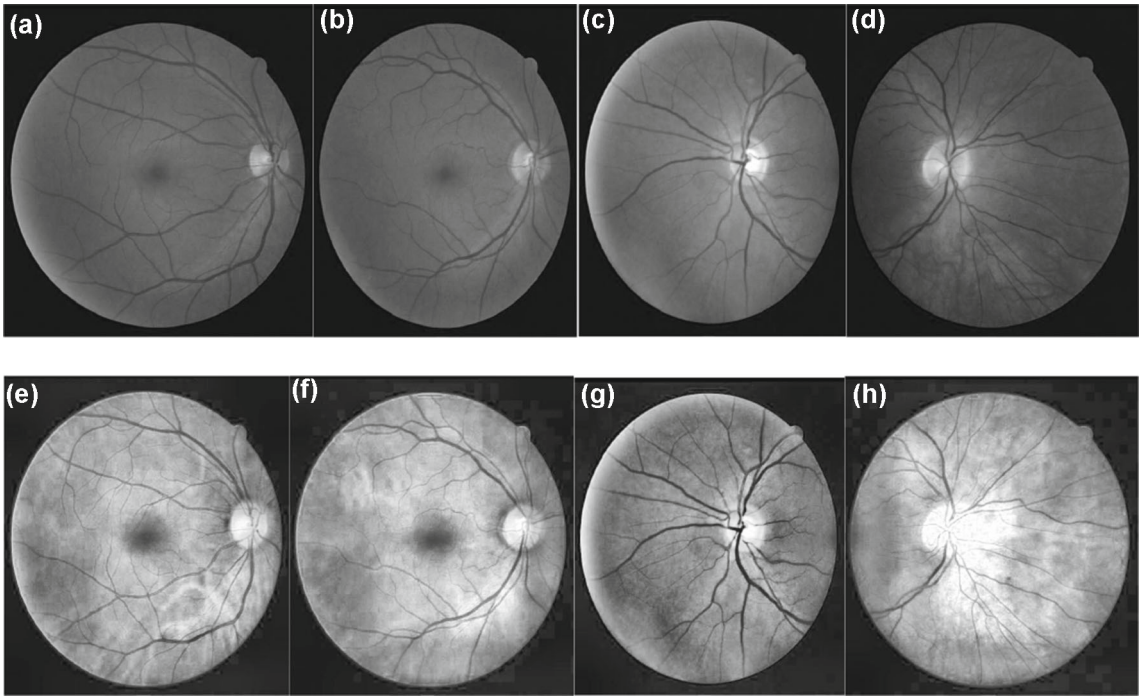

Fig. 9 **a**–**d** Green channel retinal images. **e**–**h** Corresponding contrast-enhanced images

Table 1 Image enhancement results for the retinal images

Quantitative parameter	Mean value
PSNR	29.7
CI	1.14

3.2 Pre-processing results

To significantly reduce the intra- and inter-image variability, color normalization is performed. A standard reference retinal image is used for altering the histogram of the color-distorted image. Figure 8 shows the original and the normalized images and the respective histogram. It can be clearly seen that color normalization has produced a significant positive change in the color-distorted image.

The contrast-enhanced retinal grayscale images after color normalization are illustrated in Fig. 9.

Table 1 gives the PSNR and CI values obtained. The value of the PSNR obtained is acceptable with noise removed to a greater extent.

3.3 Region of interest extraction results

As mentioned in Sect. 2.4, to extract border and optic disk morphological operations are being used. Figure 10 depicts the extracted border and optic disk. It can be clearly seen that circular border and the optic disk are clear been detected using the proposed method. Figure 12 shows the

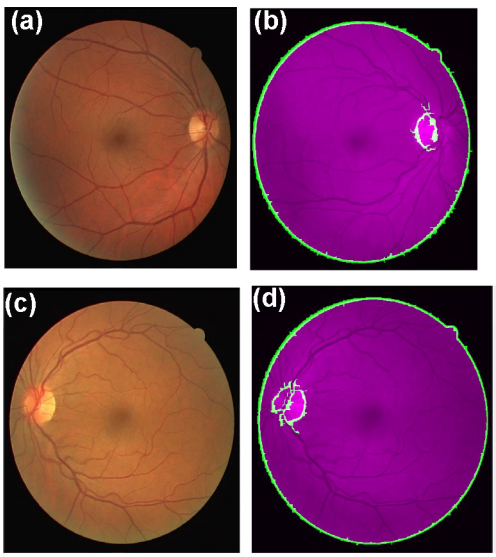

Fig. 10 Optic disk and border extraction. **a**, **c** Original fundus images. **b**, **d** Extracted border and optic disk of the images on the *left side*

extracted retinal vessels from the fundus images using DRIVE database. A structuring element with disk shaped of radius 10 units is used. According to the results obtained, it is inferred that accuracy changes dramatically as the size of structuring element is modified. Similarly, the choice of the value for neighborhood pixel for removing small unconnected components involved several iteration

A larger or small value resulted in an increase in the number of true negatives and false positives, respectively.

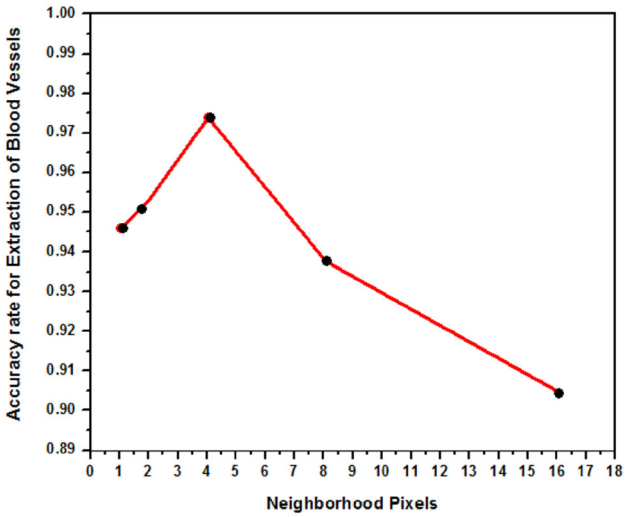

Fig. 11 Graph indicating the dependency relationship between neighborhood pixel choice and accuracy rate for extraction of blood vessels

Therefore, the optimal value is considered as four. Figure 11 shows the graph illustrating the effect of choice of neighborhood pixel on the accuracy rate. The proposed vessel extraction algorithm resulted in an accuracy of 97.22% (Fig. 12).

3.4 Comparative analysis

Staal et al. [21] developed a framework that develops wherein image ridges coinciding approximately with vessel centerlines were extracted. Every picture pixel is assigned to the most proximate line element, and the procedure is reiterated for the enter image. Each line component constitutes a nearby co-ordinate frame for its relating patch. For each individual pixel, 27 features were computed and consequently the features that exhibited the best line separability were selected utilizing sequential forward feature selection and relegated utilizing k-NN classifier. The piecewise linear property of shape features of retinal vessels was exploited by Mendonca et al. [22] by using mathematical morphology in conjunction with the iterative region growing method for vessel segmentation. A simple method of classification and post-processing was used by Marin et al. by extracting a 7D feature vector and feeding it to the neural network. The gaps in the blood vessels were filled by iterative filling algorithm with six neighboring pixels [23]. In [24], segmentation of blood vessels is performed using multi-scale feature extraction. Information pertaining to vessel topology is obtained using first and second spatial derivatives. The region growing procedure successively segments the blood vessels using feature and spatial information. Zhao et al. proposed a method based on region growing and region-based active contour with level set method to extract the blood vessels [3]. The major limitation of this method is that for abnormal retinal images the segmentation results are inaccurate due to the movement of the active contour toward pathological region. In [25], matched filter first-order derivative of Gaussian (MF-FDOG), the vessels are distinguished by applying threshold to the retinal response image. However, the resultant vessel image is inefficiently segmented due to the logical OR operation used. An improved morphology-based blood ves-

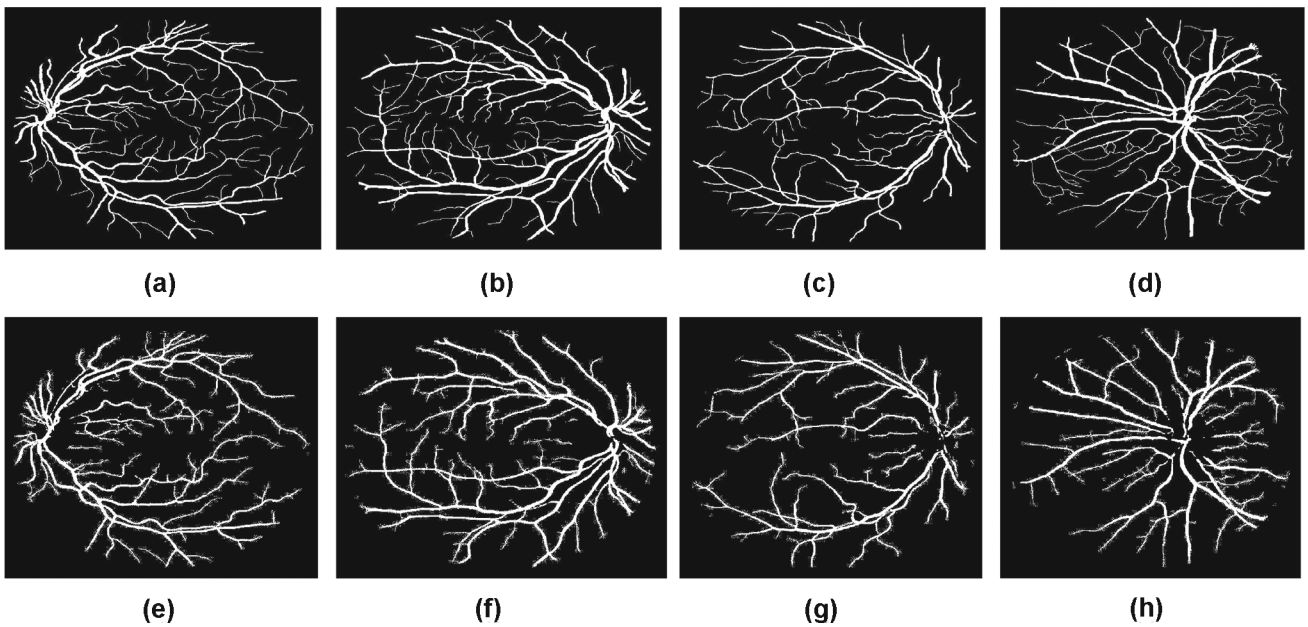

Fig. 12 Comparison of the extracted retinal vessels with corresponding gold-standard images. **a**–**d** Gold-standard images. **e**–**h** Retinal vessels obtained using proposed method

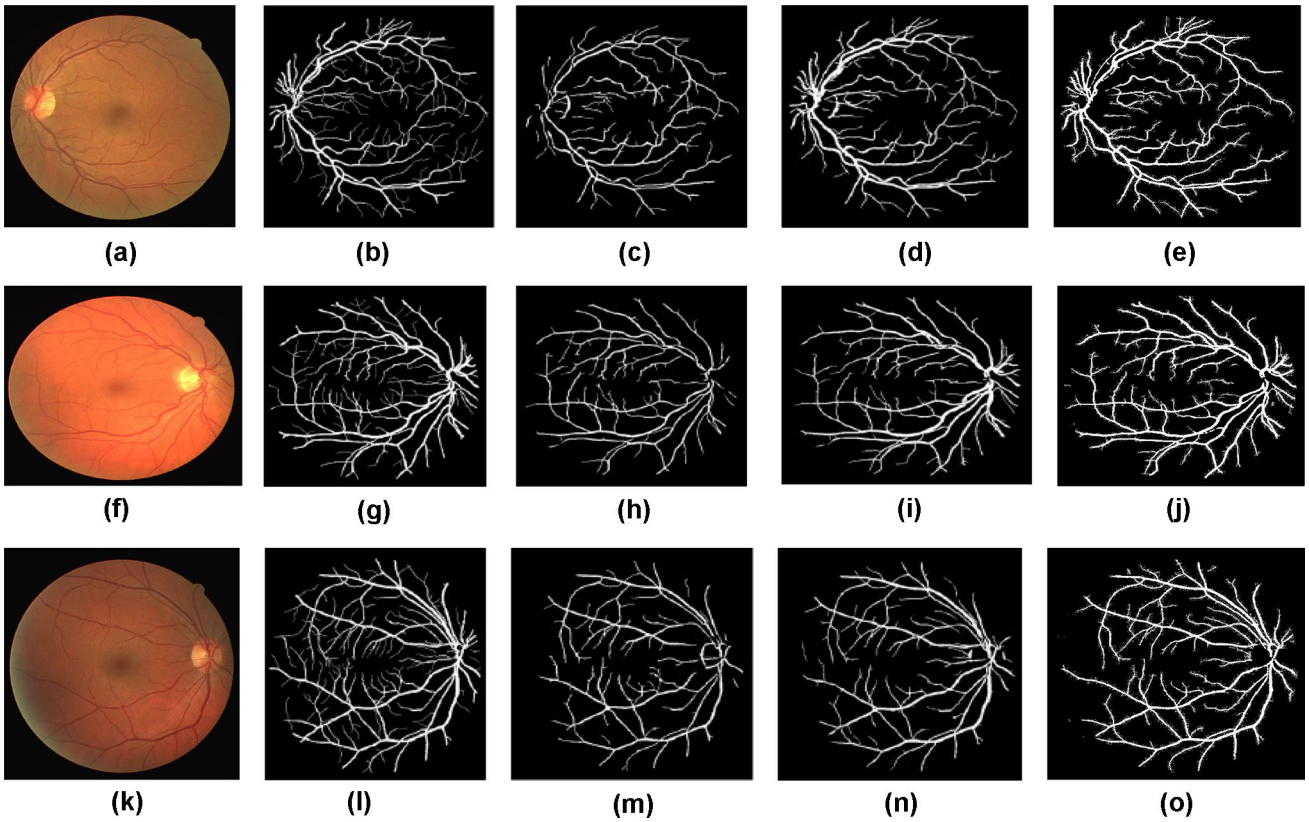

Fig. 13 Segmentation results of retinal images from the DRIVE database using different methods. The *first column* three original retinal images. The *second column* manual segmentation results. The *third* and *fourth columns* segmentation results of the MF-FDOG method [25] and the method in [3], respectively. The *last column* segmented results of the proposed method

Table 2 Comparative analysis of the proposed method with

Method	Sensitivity	Specificity	FPR	Accuracy
Human observer [16]	0.797	0.972	0.027	0.9473
[28]	0.8319	0.960	0.04	0.9535
[30]	0.276	0.997	0.003	0.903
[31]	0.714	0.949	0.051	0.918
[1]	0.719	0.972	0.028	0.939
[24]	0.796	0.961	0.039	0.939
[21]	0.778	0.971	0.029	0.946
[32]	0.773	0.975	0.025	0.949
[23]	–	–	–	0.9448
[22]	0.7344	0.9764	0.0236	0.9452
[24]	0.7505	0.9562	0.0438	–
[3]	0.7354	0.9789	0.0211	0.9477
[25]	0.7171	0.9753	0.0247	0.9483
[26]	0.7612	0.9608	0.0392	0.9458
[27]	0.7512	0.9684	0.0316	0.9412
[29]	0.725	0.983	0.017	0.952
[33]	0.7655	0.9704	–	0.9442
[34]	0.7861	0.9712	–	0.9466
Proposed method	0.8512	0.9857	0.0117	0.9722

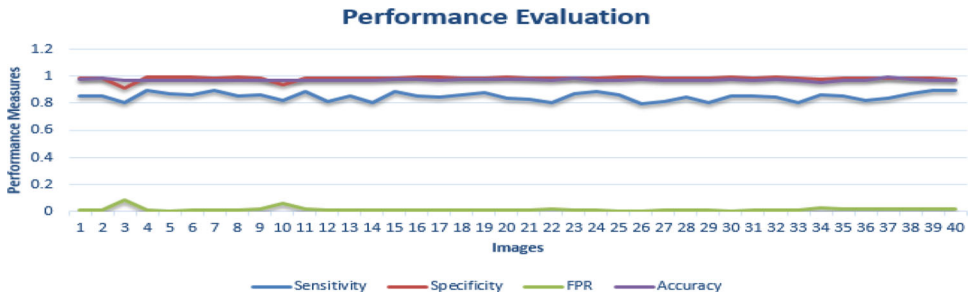

Fig. 14 Sensitivity, specificity, FPR and accuracy obtained for the images from DRIVE database

sel extraction algorithm using curvelet transform and PCA is proposed by Saleh. The method uses CCA followed by adaptive filtering in order to remove the frills and evacuate the arterioles in the image [26]. A graph cut technique is used for the extraction of retinal vessels. The segmentation of optic disk is done using Markov random field (MRF) image reconstruction as well as compensation factor method using empirical knowledge of local intensities of the retinal vessels [27]. Zhu et al. used an ensemble method based on supervised learning 36-dimensional feature vectors with multi-scale and multi-orientation, and divergence of vector field is extracted. Classification and regression tree (CART) and AdaBoost classifier are constructed iteratively by using the feature vectors as the input to perform retinal segmentation [28]. In [29], major vessels are extracted and classified based on the regions common to thresholded versions of high-pass-filtered image.

The fundus image simultaneously undergoes high-pass filtering and morphological reconstruction followed by thresholding. The vessels common to the two images are extracted and classified. The Gaussian mixture model is used as classifier taking eight features as the input. Figure 13 illustrates the results obtained by Zhang et al. [25] and Zhao et al. [3] and the proposed method with respect to the gold standard. The measurements for comparisons used are same as used by numerous authors in the literature. Table 2 shows the performance comparisons of the retinal vessel segmentation using different techniques on the DRIVE database. It can be observed that the proposed algorithm resulted in a higher accuracy of 0.9722, sensitivity of 0.8512, specificity of 0.9857 and FPR of 0.0117, which is comparably higher than the results from the existing literature and benchmark results from DRIVE database. Figure 14 shows the accuracy, sensitivity, specificity and FPR obtained. It can be clearly seen that higher values of accuracy are obtained. In our algorithm, the two-stage pre-processing technique applied in the algorithm effectively omits the artifacts and equalizes the intensity variations and then the modified Gabor filter functions introduced with automatic GLCM-based thresholding scheme without much difficulty extract the blood vessels at all orientations from the retinal image. The proposed border and optic disk extraction techniques adds to the accuracy of the overall methodology. Finally, in the subsequent stages morphology-based binarization and CCA analysis techniques efficiently eliminate the noise in the vessel extracted images. It can be inferred from our experimentation that an increase in the quantitative number of Gabor filter banks did not significantly improve the enhancement performance but caused an increase in the computational complexity. The color normalization technique and adaptively increasing the contrast of the green channel image increase the speed of the system considerably and also resulted in an increase in the accuracy of the proposed algorithm.

A Matlab prototype was utilized for implementing the proposed algorithm. The simulations run took an average processing time of 4 s for single image utilizing a medium size computer (2.93 GHz Intel Core2Duo CPU and 2 GB RAM).

4 Conclusion

The problem of extracting the useful information from the retinal images is a major task , and thus digital retinal imaging plays a major role in diagnosing retinal disorders. The experimental results indicate that Gabor filter provided good result since there is excellent localization in the frequency domain as well as space domain. The modified Gabor filter functions tuned to appropriate frequency and orientation aided in enhancing vessels along all the direction and simultaneously filtering the undesirable components. The enhanced retinal vessels are subjected to automatic thresholding for classification of the vessel pixels. GLCM provided the information regarding the gray level frequency and edge information that served the basis for entropy thresholding. Based on the fact that the brightest part in the image is the optic disk, experimentally an optimal threshold is identified for the extraction and elimination of the optic disk. It is important to notice that the performance evaluation parameters assessing the agreement of individual pixel classification indicate an average accuracy, sensitivity, and specificity of 0.9722, 0.8512, and 0.9857, respectively. The results obtained are comparably higher than those reported in the literature. One of the signif-

icant central issues in the field of restorative imaging is the lack of precise and adequate automated computer-based system for extraction of retinal features from fundus images. The system should avoid user intervention and be robust enough to analyze different kinds of images. This involves a large challenge within the field of retinal imaging. The proposed method can be a helping hand to assist ophthalmologists for analyzing fundus images in order to assess eye disorders.

Acknowledgements The authors express their gratitude to Prof. Tanweer, REVA University Bangalore, for his extensive support and contribution in carrying out this research. This work was supported by Manipal University Dr. T.M.A. Pai Research Scholarship under Research Registration No. 160900105-2016.

References

1. WHO Global Report on Diabetes. http://www.who.int/diabetes/global-report/en/
2. Moghimirad, E., Rezatofighi, S.H., Soltanian-Zadeh, H.: Multiscale approach for retinal vessel segmentation using medialness function. In: IEEE International Symposium on Biomedical Imaging: From Nano to Macro, pp. 29–32 (2010)
3. Zhao, Y.Q., Wang, X.H., Wang, X.F., Shih, F.Y.: Retinal vessels segmentation based on level set and region growing. Pattern Recognit. **47**(7), 2437–2446 (2014)
4. Staal, J., Abramoff, M.D., Niemeijer, M., Viergever, M.A., van Ginneken, B.: Ridge-based vessel segmentation in color images of the retina. IEEE Trans. Med. Imaging **23**(4), 501–509 (2004)
5. Sofka, M., Stewart, C.V.: Retinal vessel centerline extraction using multiscale matched filters, confidence and edge measures. IEEE Trans. Med. Imaging **25**(12), 1531–1546 (2006)
6. Odstrcilik, J., Kolar, R., Budai, A., Hornegger, J., Jan, J., Gazarek, J., Kubena, T., Cernosek, P., Svoboda, O., Angelopoulou, E.: Retinal vessel segmentation by improved matched filtering: evaluation on a new high-resolution fundus image database. IET Image Proc. **7**(4), 373–383 (2013)
7. Zhang, J., Dashtbozorg, B., Bekkers, E., Pluim, J., Duits, R., ter Haar Romeny, B.: Robust retinal vessel segmentation via locally adaptive derivative frames in orientation scores. IEEE Trans. Med. Imaging **35**(12), 2631–2644 (2016)
8. Vlachos, M., Dermatas, E.: Multi-scale retinal vessel segmentation using line tracking. Comput. Med. Imaging Graph. **34**(3), 213–227 (2010)
9. Yin, Y., Adel, M., Bourennane, S.: Retinal vessel segmentation using a probabilistic tracking method. Pattern Recognit. **45**(4), 1235–1244 (2012)
10. De, J., Ma, T., Li, H., Dash, M., Li, C.: Automated tracing of retinal blood vessels using graphical models. In: Scandinavian Conference on Image Analysis. Springer, Berlin (2013)
11. Cheng, J., Liu, J., Xu, Y., Yin, F., Wong, D.W., Tan, N.M., Tao, D., Cheng, C.Y., Aung, T., Wong, T.Y.: Superpixel classification based optic disc and optic cup segmentation for glaucoma screening. IEEE Trans. Med. Imaging **32**(6), 1019–1032 (2013)
12. Aquino, A., Gegundez-Arias, M.E., Marin, D.: Detecting the optic disc boundary in digital fundus images using morphological, edge detection, and feature extraction techniques. IEEE Trans. Med. Imaging **29**(11), 1860–1869 (2010)
13. Morales, S., Naranjo, V., Angulo, J., Alcaniz, M.: Automatic detection of optic disc based on PCA and mathematical morphology. IEEE Trans. Med. Imaging **32**(4), 786–96 (2013)
14. Alshayeji, M., Al-Roomi, S.A., Abed, S.E.: Optic disc detection in retinal fundus images using gravitational law-based edge detection. Med. Biol. Eng. Comput. **55**(6), 935–948 (2016)
15. Pereira, C., Gonçalves, L., Ferreira, M.: Optic disc detection in color fundus images using ant colony optimization. Med. Biol. Eng. Comput. **51**(3), 295–303 (2013)
16. DRIVE: Result Browser. http://www.isi.uu.nl/Research/Databases/DRIVE/browser.php. Accessed 3 Jan 2017
17. Gabor, D.: Theory of communication. Part 1: the analysis of information electrical engineers—part III. J. Inst. Radio Commun. Eng. **93**(26), 429–41 (1946)
18. Liu, Z.Q., Cai, J., Buse, R.: Hand-Writing Recognition: Soft Computing and Probablistic Approaches. Springer, Berlin (2003)
19. Gonzalez, R.C., Woods, R.E.: Digital image processing (2008)
20. Jain, A.: Fundamentals of Digital Image Processing. Prentice-Hall, Englewood Cliffs (1986)
21. Staal, J.J., Abramoff, M.D., Niemeijer, M., Viergever, M.A., Van Ginneken, B.: Ridge based vessel segmentation in color images of the retina. IEEE Trans. Med. Imaging **23**, 501–509 (2004)
22. Mendonca, A.M., Campilho, A.: Segmentation of retinal blood vessels by combining the detection of centerlines and morphological reconstruction. IEEE Trans. Med. Imaging **25**(9), 1200–1213 (2006)
23. Marin, D., Aquino, A., Gegundez-Arias, M.E., Bravo, J.M.: A new supervised method for blood vessel segmentation in retinal images by using gray-level and moment invariants-based features. IEEE Trans. Med. Imaging **30**(1), 146–58 (2011)
24. Martinez-Perez, M.E., Hughes, A.D., Thom, S.A., Bharath, A.A., Parker, K.H.: Segmentation of blood vessels from red-free and fluorescein retinal images. Med. Image Anal. **11**(1), 47–61 (2007)
25. Zhang, B., Zhang, L., Zhang, L., Karray, F.: Retinal vessel extraction by matched filter with first-order derivative of Gaussian. Comput. Biol. Med. **40**(4), 438–45 (2010)
26. Shahbeig, S.: Automatic and quick blood vessels extraction algorithm in retinal images. IET Image Proc. **7**(4), 392–400 (2013)
27. Salazar-Gonzalez, A., Kaba, D., Li, Y., Liu, X.: Segmentation of the blood vessels and optic disk in retinal images. IEEE J. Biomed. Health Inform. **18**(6), 1874–1886 (2014)
28. Zhu, C., Zou, B., Xiang, Y., Cui, J., Wu, H.: An ensemble retinal vessel segmentation based on supervised learning in fundus images. Chin. J. Electron. **25**(3), 503–511 (2016)
29. Roychowdhury, S., Koozekanani, D.D., Parhi, K.K.: Blood vessel segmentation of fundus images by major vessel extraction and sub image classification. IEEE J. Biomed. Health Inform. **19**(3), 1118–1128 (2015)
30. Chaudhuri, S., Chatterjee, S., Katz, N., Nelson, M., Goldbaum, M.: Detection of blood vessels in retinal images using two-dimensional matched filters. IEEE Trans. Med. Imaging **8**(3), 263–269 (1989)
31. Jiang, X., Mojon, D.: Adaptive local thresholding by verification-based multithreshold probing with application to vessel detection in retinal images. IEEE Trans. Pattern Anal. Mach. Intell. **25**(1), 131–137 (2003)
32. Zana, F., Klein, J.: Segmentation of vessel-like patterns using mathematical morphology and curvature evaluation. IEEE Trans. Image Process. **10**(7), 1010–1019 (2001)
33. Azzopardi, G., Strisciuglio, N., Vento, M., Petkov, N.: Trainable COSFIRE filters for vessel delineation with application to retinal images. Med. Image Anal. **19**(1), 46–57 (2015)
34. Zhang, J., Chen, Y., Bekkers, E., Wang, M., Dashtbozorg, B., Haar Romeny, B.M.: Retinal vessel delineation using a brain-inspired wavelet transform and random forest. Pattern Recognit. **69**, 107–123 (2017)